ACS OMEGA

http://pubs.acs.org/journal/acsodf

Article

Kinetic Study on Continuous Sampling of Coal Char from a Micro Fluidized Bed

Zehua Li,* Renjie Zou, Yang Xu, Liang Cao, Guangqian Luo,* and Hong Yao

Cite This: *ACS Omega* 2021, 6, 9086−9094

Read Online

ACCESS | Metrics & More | Article Recommendations

ABSTRACT: We self-design a micro fluidized bed reactor (MFB) with combination of an online char particle sampling system to study the kinetics of coal char combustion and gasification. The system mainly contains two parts: a micro fluidized bed and vacuum online sampling. Vientiane coal was continuously sampled from the MFB. Both combustion and gasification reactivities of the sampled chars were tested in a thermogravimetric analyzer. Kinetic parameters of the sampled char were analyzed. Char reactivity in oxy-fuel combustion in the MFB obeys the rule of decrease−increase−decrease behavior with the sampling time. Pre-exponential factor *A* and activation energy *E* of the sampled char increase with the sampling time. The gasification reactivity of the sampled char increases with the sampling time even though there is a minor decrease in an initial gasification stage. The new designed MFB combining with the online sampling system will pave the path for the investigation of gas−solid reaction evolution in the future.

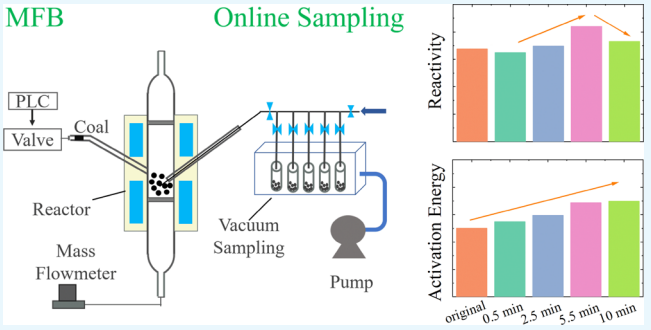

1. INTRODUCTION

Oxy-fuel combustion has many advantages over conventional air combustion.[1,2] In oxy-fuel combustion, O_2 is usually separated from air and mixed with the recycled flue gas in a power plant. CO_2 can reach as high as 95% in the flue gas, which makes CO_2 capture easier. The cyclic flue gas contains high concentration of CO_2, which is therefore compressed and stored underground. Oxy-fuel combustion has a good CO_2 capture efficiency comparing to other technologies such as absorbing CO_2 by solid sorbents.[3−5] As a result, good economic benefits can be realized in oxy-fuel combustion.[6]

Char structure evolution during combustion or gasification has been investigated by many researchers in recent years.[7−15] Char morphology and structure, i.e., size, thickness, porosity, and functional groups, have significant effects on char reactivity,[13−15] as well as other applications.[16−18]

Char is usually generated from a short pyrolysis stage in a boiler followed by combustion or gasification. Char morphology in the pyrolysis stage has been reported in our previous report[12] and hence not discussed in this study. This study investigates char morphology evolution and its impact on reactivity in the combustion and gasification stage.

During combustion, it was reported that char density and size gradually decrease,[19,20] while the char surface area increases due to the formation of a large amount of meso- and micropores.[19] However, in Liu's calculation,[20] the specific surface area shows different rules during combustion, where it either first increases to a maximum and then decreases or only decreases to the end of the combustion. Apart from physical structure evolution, a preferential loss of functional groups may affect char reactivity.[21] It is reported that char combustion reactivity decreases with the proceeding of the combustion, which is due to the loss of the intrinsic reactivity[19] as well as the functional groups like a carbonaceous matrix.[21]

During gasification, the char surface area decreased rapidly and then was kept constant. The degree of char graphitization gradually increased during gasification by *in situ* Raman spectroscopy,[22,23] which may result in the decrease in the char reactivity.

However, the char structure and reactivity evolutions during coal combustion or gasification are mostly investigated in a fixed bed or a drop furnace in the previous literature. A fixed bed reactor has disadvantages of oxygen diffusion limitation and temperature deviation for gas−solid reaction measurements. A drop furnace is usually used to measure rapid reactions at high temperature. The disadvantages of the drop furnace are that it is hard to measure a nonrapid gas solid reaction and to realize an isothermal environment due to

Received: January 8, 2021
Accepted: March 16, 2021
Published: March 24, 2021

significant reduction in radiation heat transfer at low temperature. Hence, it is a good choice to measure char structure and reactivity evolutions in an MFB reactor.

The MFB has the advantage of mass and heat transfer for isothermal reactions and has been applied to investigate the kinetic study of gas−solid reactions. We have previously used an MFB to determine coal char combustion[24−26] and gasification[27,28] as well as petroleum coke gasification,[29] which shows good reliability. Zhao et al. used an MFB to determine steam gasification of *in situ* char.[30,31] Xu et al. used an MFB to measure several kinds of gas−solid reactions.[32,33] All these studies show very good reliability of the MFB for investigating gas−solid reactions.

In this study, we propose to use the MFB reactor combining with a continuous sampling system to investigate coal char reactivity evolution during combustion and gasification. Kinetic evolution is determined by an isothermal method. This study will pave the path for online sampling in the MFB for gas−solid reactions in the future.

2. MATERIALS AND METHODS

2.1. Sample Preparation. A Vientiane coal sample was selected in this study. Raw coal was ground and sieved to a diameter of 75−100 μm. We have investigated the effect of char diameter on char conversion in such MFBs in our previous study[24] and found that the carbon conversion rate did not increase with decreasing the particle size below 100 μm, indicating that the internal diffusion limitation could be disregarded when the particle size was less than 100 μm.

Later, coal samples were put into the oven and dried at 378 K for 1 hour. The proximate and ultimate analysis are shown in our previous studies.[12,26]

2.2. Vacuum Online Sampling. In the MFB reactor, we could measure the char reactivity by detecting the outlet gas by gas chromatography (GC) and/or mass spectrometry (MS). Char reactivity identified from outlet gas measurement is the overall average reactivity, which cannot represent immediate reactivity during the reactions. Then, the question is how we can measure the immediate reactivity. Sampling a char out of the MFB reactor by an online solid particle sampling system and directly measuring its reactivity can be a good choice. To the best of our knowledge, the idea of combining the MFB with an online solid particle sampling system is first reported in this study.

We self-developed an MFB with combination of an online char particle sampling system to study coal char combustion and gasification. The schematic diagram of the experiment apparatus is shown in Figure 1, which mainly contains two parts: (left) a micro fluidized bed and (right) vacuum online sampling. The reactor in the MFB is in a dimension of 25 mm in inner diameter and 180 mm in height. Two wind boards with a distance of 50 mm in between are placed in the middle of the reactor in which char combustion takes place. The vacuum online sampling system mainly consists of a sampling tube, vacuum box, and vacuum pump. A thermocouple was placed in the sampling tube (not shown in Figure 1) to measure the temperature at the sampling point in the MFB. The vacuum box is in a dimension of 50 × 30 × 20 cm. The inner diameter of the sampling tube is 3 mm.

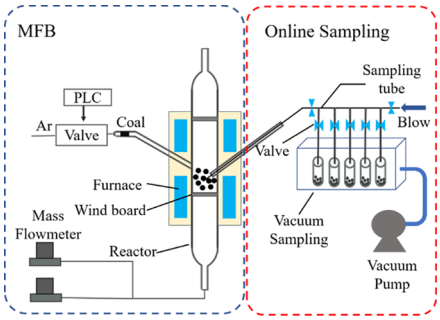

Figure 1. Schematic diagram of integration of the MFB and online sampling system.

Sampling tube is inserted to the fluidized zone in the MFB. All valves were closed, and the sampling box was vacuumed to the pressure as lowest as 0.09 MPa within 10 s before starting online char sampling. Char particles were sampled at different reaction times to different bottles located in the sampling box by opening the corresponding valve. Once sampling was finished, a flow of cold Ar was injected to the sampling tube and sampling bottle to cool the sampled char. The cooled char was then collected for further analysis.

There are some other techniques solving the immediate reactivity during the reaction. For instance, a spatially resolved reactor was designed to solve intermediate reactions, catalyst structure evolutions, and subkinetic parameters from different parts along the axial in the sample bed.[34−36] In this technique, the reactor involves reactants flowing through a solid catalyst bed containing a sampling capillary with a side sampling orifice, where a very small amount of *in situ* gas is sampled and transferred into an analytical device (GC/MS) for quantitative analysis. The sampling capillary can be moved with μm resolution in or against the flow direction to measure species profiles through the catalyst bed. Some other researches propose to solve immediate species and structures by a so-called spatially resolved infrared radiation (IR) surface analysis by continuously moving a fixed bed.[37] However, all these techniques are measured from the fixed bed and have their own disadvantages.

2.3. Experimental Procedure. Raw coal was first pyrolyzed in a fixed reactor at 1173 K in an Ar atmosphere for 4 h to deeply remove the volatile. The pyrolysis experimental setting can be found in our previous study.[12]

For combustion in the MFB, the temperature was set to 823 K. A stream with 125 mL/min O_2 and 375 mL/min CO_2 was injected to the reactor. The sampling box was vacuumed to 0.09 MPa. The char sample (1 g) was then fed to the MFB by a programmable logical controller (PLC)-controlled Ar pulse after stabilization of temperature and flow stream. Open electromagnetic valve to start sampling at 0.5, 2.5, 5.5 and 10 min, respectively. The sampled char was collected (10−20 mg) and cooled down in the sample bottles, which were placed in the vacuum box. Sampled char surface morphology was measured by field emission scanning electron microscopy (FESEM) with a resolution of 0.8 nm (GeminiSEM 300).

Generally, it is better to use a milligram char sample in kinetic studies in the MFB. However, we have to sample the char particles as enough as possible out of the MFB at different reaction stages to further determine their kinetic parameters in a thermogravimetric analyzer (TGA). We have tried the experiments with the char sample of milligrams, and few char particles were sampled out and not enough to measure the kinetics in the later thermogravimetric (TG) experiment. Comparing with char sample in milligrams, we do not think

https://doi.org/10.1021/acsomega.1c00131
ACS Omega 2021, 6, 9086−9094

the char sample mass (1 g) will affect the properties of the char because our char particles are totally fluidized in the MFB.

For gasification in the MFB, the temperature was set to 1123 K. Gasification is an endothermic reaction. It requires heat to start up and a long time to operate the gasification furnace in industrial application. The heat could be from the combustion reaction with supplying of low concentration of O_2 (char−O_2 reaction). Although in an experimental scale we electrically heat the reactor, we still add a low concentration (5%) of O_2 to the reaction atmosphere to simulate the case in industrial application. In this way, we still call it gasification. Experimentally, a stream with 25 mL/min O_2, 300 mL/min CO_2, and 175 mL/min steam was injected to the reactor. The sampling times selected were 0.5, 1.0, 1.5, and 2.0 min. Other experimental settings are the same with the combustion experiment.

2.4. Kinetic Determination. The reactivity of sampled char from combustion in the MFB was determined in a TGA (STA 449 F3) at 773, 823, and 873 K in an O_2/Ar atmosphere (21 mL/min O_2, 79 mL/min Ar). TGA temperature was first increased to the target temperature at a rate of 10 K/min in an Ar atmosphere. The atmosphere was then shifted to O_2/Ar after temperature stabilization. In each measurement, the mass of the sampled char was 5 mg. The mass loss was continuously recorded.

The reactivity of sampled char from gasification in the MFB was determined in the same TGA at 1273 K but with a vapor furnace reactor. Temperature was set from 423 to 1273 K at a heating rate of 20 K/min in an N_2 atmosphere. Then, a stream of mixed CO_2, steam and N_2 with varied concentrations was injected to the reactor.

Kinetic determination of char oxidation (combustion and gasification) can be found in our previous study.[12,26,38] The char conversion X is calculated by the weight loss data as eq 1:

$$X = \frac{m_0 - m_t}{m_0 - m_\infty} \tag{1}$$

where m_0, m_t, and m_∞ represent the initial mass of char sample, mass of the sample at reaction time t, and mass of the sample when the reaction was finished, respectively.

In this study, the reactivity index R_s (min^{-1}) was defined as eq 2 to evaluate the overall char reactivity.[29,39] $t_{0.5}$ is the time required to reach the char conversion of 50%.

$$R_s = \frac{0.5}{t_{0.5}} \tag{2}$$

The reaction rate constant k can be calculated as follows:

$$\frac{d_X}{d_t} = kf(X) \tag{3}$$

where $f(X)$ is the reaction model function. The integral format of $f(X)$ can be described as eq 4:

$$G(X) = \int_0^X \frac{1}{f(X)} d_X = \int_0^t k d_t = kt \tag{4}$$

Therefore, the reaction rate constant can be calculated because there is a linear relationship between $G(X)$ and t in the isothermal experiments. The reaction rate constant k is the slope of the fitting straight line.

If the main intention for studying coal reactivity is just to describe the relation between time and conversion, a shrinking core model is preferred.[40] The shrinking core model fits the results well from our previous work[12,38] and other researcher's publications.[41,42] The shrinking core model (eq 5) is selected as the mechanism function model in this study because of its mathematical simplicity, and the conversion time behavior is well described.

$$G(X) = 1 - (1 - X)^{1/2} \tag{5}$$

As a comparison, the other two models, nucleation and growth model and two-dimensional diffusion model, are calculated from $G(X)$ expressed as eqs 6 and 7, respectively.

$$G(X) = -\ln(1 - X) \tag{6}$$

$$G(X) = X + (1 - X)\ln(1 - X) \tag{7}$$

After the calculation of reaction rate constant k under different temperatures, the following eq 8 is then straight forward according to the Arrhenius equation:

$$\ln k = \ln A - E/RT \tag{8}$$

The plot ($\ln k$, $1/T$) fits on a straight line. The activation energy $-E/R$ and pre-exponential factor $\ln A$ are the slope and the intercept, respectively.

3. RESULTS AND DISCUSSION

3.1. Online Sampling Char Morphology. Surface morphologies of the sampled char at different times are shown in Figure 2. On the original char surface, there are few fissures and micropores but they are not obvious (Figure 2a), which is perhaps due to the long-time pyrolysis at high temperature in the fixed bed to deeply remove the volatile content from raw coal. High temperature could result in a slight sintering. In the early combustion stage, there are some micropores and small char particles on the surface of the sampled char at 0.5 min (Figure 2b). In this stage, char was

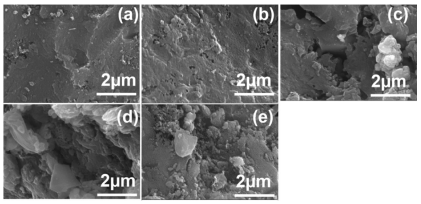

Figure 2. FSEM images of the online sampled char morphology: (a) original char, (b) 0.5, (c) 2.5, (d) 5.5, and (e) 10 min.

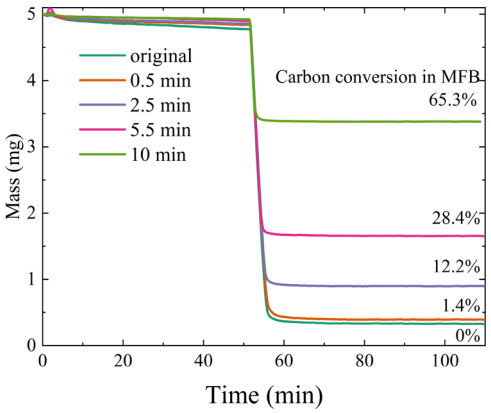

Figure 3. Carbon conversion in the MFB at different sampling times.

https://doi.org/10.1021/acsomega.1c00131
ACS Omega 2021, 6, 9086−9094

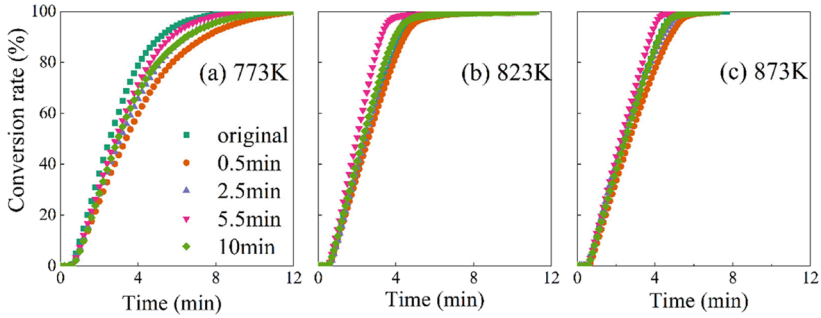

Figure 4. Combustion conversion of the sampled char at different temperatures: (a) 773, (b) 823, and (c) 873 K.

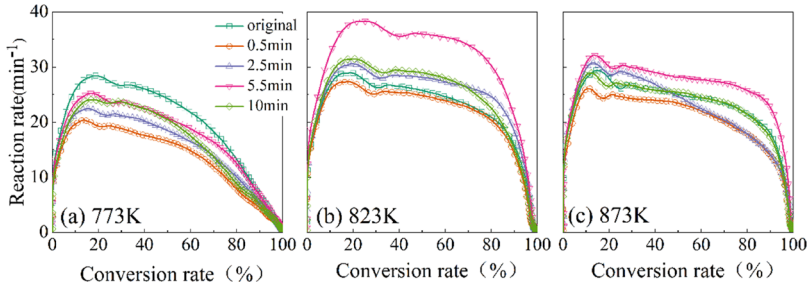

Figure 5. Combustion reaction rate of the sampled char at different temperatures: (a) 773, (b) 823, and (c) 873 K.

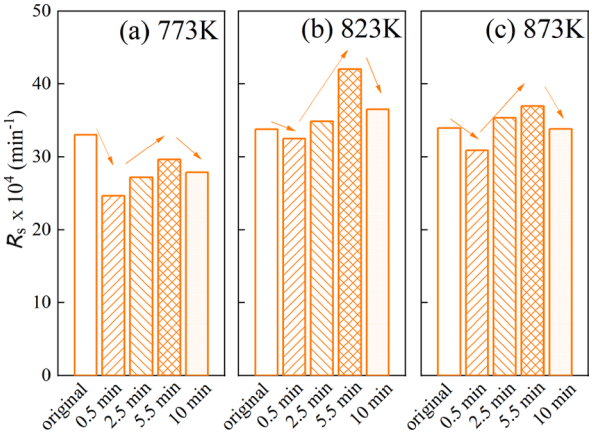

Figure 6. Reactivity index R_s of the sampled char at different temperatures: (a) 773, (b) 823, and (c) 873 K.

heated from room temperature to experimental high temperature (823 K) in an O_2/CO_2 atmosphere. Both heating and oxidant could make char particle active, and active sites on char surface were first consumed in the short reaction time. In the middle combustion stage, macropore occurs, and char pores become much developed (pore enlargement) with char combustion proceeding at 2.5 and 5.5 min (Figure 2c,d). In this stage, O_2/CO_2 further diffused into the internal of the char particle, and most of carbon was consumed, which resulted in the pore enlargement. The middle combustion stage takes about 50−70% of the whole combustion process, and the reaction rate is much stable,[12] which is the best stage to determine char kinetic parameters. Details will be discussed in later sections. In the late combustion stage, macropore breaks and collapses on the surface of the sampled char at 10 min, where most of carbon was consumed and coal ash left (Figure 2e). In this stage, coal ash blocked oxidant diffusion especially when coal ash melt, which resulted in the decrease of combustion rate.

3.2. Char Combustion Reactivity. The combustion reactivity of the online sampled chars was measured in a TGA. Typical TG curves are shown in Figure 3 from which the carbon conversion in the MFB is calculated. The total carbon in the original char is calculated from $\Delta m_{original} = m_0 - m_\infty$, and the resident carbon in the sampled char is $\Delta m_t = m_0 - m_\infty$. m_0 and m_∞ represent the initial and final sample mass in TGA, respectively. Therefore, the carbon conversion of the sampled char in the MFB could be calculated as $X = \frac{\Delta m_{original} - \Delta m_t}{\Delta m_{original}}$, and the final conversions of the sampled char are shown in Figure 3. The carbon conversion is from 1.4 to 65.3% for the sampled char from sampling time of 0.5 to 10 min.

Char conversion (X) and reaction rate (dX/dt) versus oxidation time are shown in Figure 4. Char conversion rate is enhanced with increasing temperature. For example, it takes about 12 min to finish combustion at 773 K, while only 5 min is required at 873 K. Further, we can see that the conversion rate of the sampled char shows nonmonotonic behaviors with the sampling time. This is the main finding in our study, which will be discussed in more detail in later sections.

Figure 5 shows the reaction rate of different sampled chars. Obviously, char has different reaction rates in different combustion stages (reaction time) with an increase−stable−decrease feature. In early combustion stage (i.e., carbon conversion rate <10%), the reaction rate decreases from the original char (square) to 0.5 min sampling char (circle). In the middle combustion stage (i.e., carbon conversion rate 10−60%), it increases from 0.5 min sampling char to 5.5 min sampling char (down triangle). In the late combustion stage (i.e., carbon conversion rate >60%), it decreases from 5.5 min sampling char to 10 min sampling char (diamond). Sampled char reactivity is sensitive to measuring temperature in TG, where sampled char at 5.5 min shows at the highest reaction rate at 823 and 873 K.

Reaction rate curves in Figure 5 show the information for the whole conversion range from 0 to 100%, while reaction

https://doi.org/10.1021/acsomega.1c00131
ACS Omega 2021, 6, 9086−9094

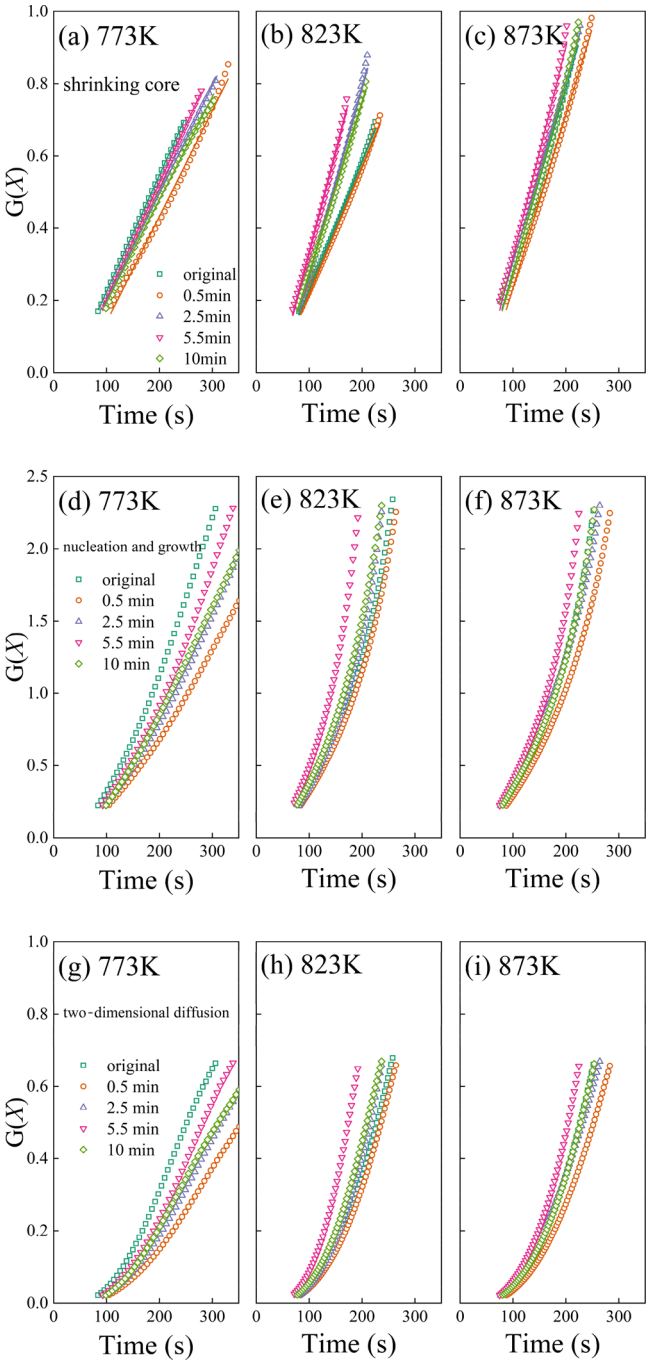

Figure 7. Linear fitting of G(X) vs reaction time using three different models: (a–c) shrinking core model, 773, 823, and 873 K; (d–f) nucleation and growth model, 773, 823, and 873 K; and (g–i) two-dimensional diffusion model, 773, 823, and 873 K.

index R_s shows the overall average char reactivity as shown in Figure 6. Similarly, it also shows that char reactivity obeys the rule of decrease–increase–decrease behavior along with the sampling time.

.

For the original char, the carbon structure is much disordered from a Raman spectrometer, which will be detailedly presented in our further report. Although there are some small pore openings in the 0.5 min sampling char (Figure 2b), char quickly tends to ordered from original char to 0.5 min sampling char in the early combustion stage. Therefore, the reactivity of 0.5 min sampling char is lower than original char (Figure 6). However, the disordered char structure will not dominate in later combustion. The pore structure and carbon matrix will dominate in the middle combustion stage, while the ash component will dominate in the late combustion stage. With pores developing from 0.5 to 5.5 min (Figure 2b–d), both reaction contact area and carbon active sites increase, leading to the increase in char reactivity (Figure 6). However, at the late combustion stage, pore structure collapses, and the ash component blocks the pore path (Figure 2e), which reduces the char reactivity (Figure 6).

Table 1. Reaction Rate Constants and Kinetic Parameters of the Sampled Char Calculated from the Shrinking Core Model

sampling time	T (K)	R^2	k (s^{-1})	ln k	A (s^{-1})	E (kJ/mol)
original	773	0.9999	0.00322	−5.738	0.153	25.05
	823	0.9979	0.00357	−5.635		
	873	0.9948	0.00506	−5.286		
0.5 min	773	0.9938	0.00293	−5.833	0.204	27.40
	823	0.9972	0.00352	−5.649		
	873	0.9966	0.00479	−5.341		
2.5 min	773	0.9999	0.00298	−5.816	0.336	29.79
	823	0.9950	0.00521	−5.257		
	873	0.9989	0.00501	−5.296		
5.5 min	773	0.9999	0.00319	−5.748	0.726	34.38
	823	0.9957	0.00558	−5.189		
	873	0.9938	0.00583	−5.145		
10 min	773	0.9980	0.00284	−5.864	0.684	34.89
	823	0.9967	0.00473	−5.354		
	873	0.9945	0.00525	−5.250		

3.3. Char Combustion Kinetic. G(X) fittings versus oxidation time calculated from three different models are shown in Figure 7 at the range of conversion rate from 0.1 to 0.9. Overall, the shrinking core model fits the experiment well at the measured temperatures for different sampled chars (Figure 7a–c). However, the nucleation and growth model (Figure 7d–f) and two-dimensional diffusion model (Figure 7g–i) fail to fit as a straight line particularly at a low conversion rate. That is to say that the shrinking core model is better than the nucleation and growth model and two-dimensional diffusion model to fit char combustion in the TG reactor. Therefore in later sections, we used the shrinking core model to calculate kinetic parameters. The reaction rate constant k is the slope of the fitting straight line from the shrinking core model (Figure 7a–c).

Table 1 shows the value of the reaction rate constant measured at various temperatures for the sampled chars. R^2 from the fittings are over 0.99, which indicates the reliability of the fittings. For a specific char, either original char or the sampled char, reaction rate constant k increases with the increase in temperature. Take the sampled char at 10 min for example, the reaction rate constant increases from 0.00284 to 0.00525 s^{-1} with increasing temperature.

When comparing the reaction rate constant between original and different sampled chars, it obeys the rule of decrease–increase–decrease behavior with the sampling time. For example, at 773 K, the reaction rate constants are 0.00322 s^{-1} (original char), 0.00293 s^{-1} (0.5 min sampling char), 0.00298 s^{-1} (2.5 min sampling char), 0.00319 s^{-1} (5.5 min sampling char), and 0.00284 s^{-1} (10 min sampling char).

https://doi.org/10.1021/acsomega.1c00131
ACS Omega 2021, 6, 9086–9094

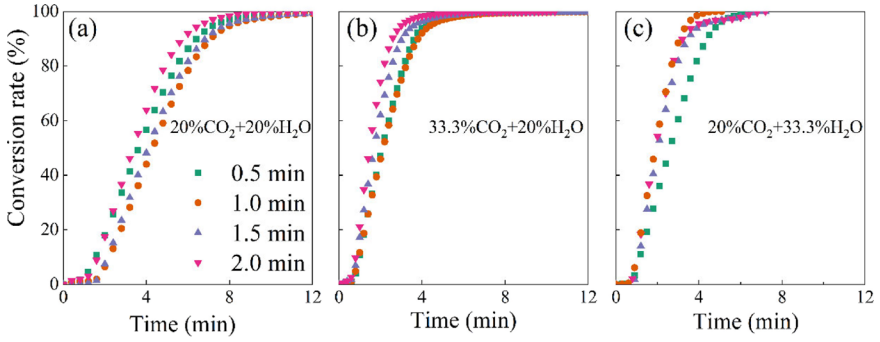

Figure 8. Gasification conversion of the sampled char at different gasification atmospheres: (a) 20% CO_2 + 20% H_2O, (b) 33.3% CO_2 + 20% H_2O, and (c) 20% CO_2 + 33.3% H_2O.

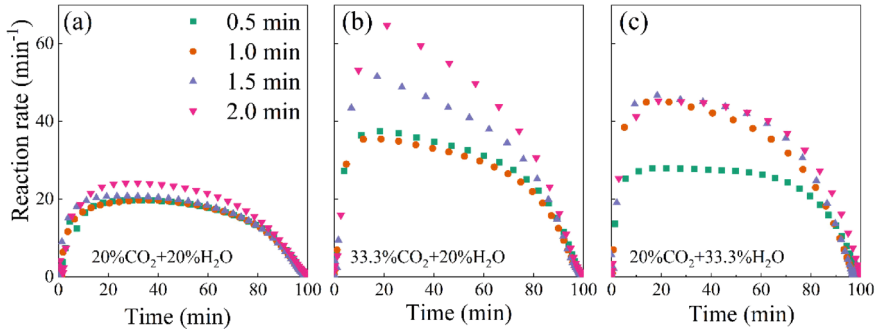

Figure 9. Gasification rate of the sampled char at different gasification atmospheres: (a) 20% CO_2 + 20% H_2O, (b) 33.3% CO_2 + 20% H_2O, and (c) 20% CO_2 + 33.3% H_2O.

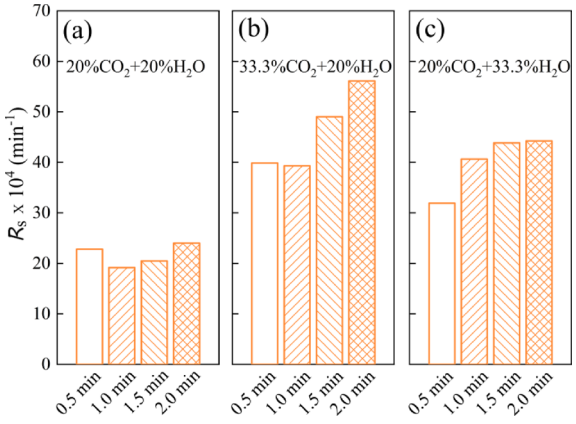

Figure 10. Reactivity index R_s of the sampled char at different gasification atmospheres: (a) 20% CO_2 + 20% H_2O, (b) 33.3% CO_2 + 20% H_2O, and (c) 20% CO_2 + 33.3% H_2O.

Table 2. Reaction Rate Constants of the Sampled Char (Calculated from the Shrinking Core Model)

	k (s^{-1})		
sampling time	20% CO_2 + 20% H_2O	33.3% CO_2 + 20% H_2O	20% CO_2 + 33.3% H_2O
0.5 min	0.00225	0.00403	0.00343
1.0 min	0.00220	0.00363	0.00400
1.5 min	0.00221	0.00442	0.00431
2.0 min	0.00260	0.00556	0.00530

Reaction rate constant decreases first from original char to 0.5 min sampling char, followed by increasing from 0.5 min sampling char to 5.5 min sampling char. Finally it decreases again to 10 min sampling char. The similar results could be also found in other temperatures, which agree with the results in Figure 6.

When the values of k at different temperatures were determined, and the kinetic parameters could be obtained according to eq 8. The values of ln k at different cases are listed in Table 1, as well as the calculated values of pre-exponential factor A and activation energy E. Both pre-exponential factor A, i.e., from 0.153 to 0.684 s^{-1}, and activation energy E, i.e., from 25.05 to 34.89 kJ/mol, of the sampled char increase with the sampling time, which is much different from the rule of char reactivity (Figure 6). This indicates that the sampled char reactivity is determined by not only kinetic parameters but also the char structure (i.e., pore structure and carbon matrix). A high pre-exponential factor means high molecule collision. High activation energy results in the reaction taking place difficulty. With the combustion proceeding in the MFB, coal char becomes more and more reactive because of the increase of pre-exponential factor A. However, because the char structure becomes ordered and activation energy increases, char reactivity slightly decreases at the early combustion stage (≤0.5 min in this study). In late combustion stage, the activation energy has a little change from 5.5 to 10 min sampling char. However, due to the pore collapse and ash blocking, char reactivity decreases at the end (Figure 6).

3.4. Char Gasification Reactivity. Coal char was continuously sampled in CO_2/H_2O gasification atmospheres. Char gasification conversion (X) and reaction rate (dX/dt) are shown in Figure 8. Compared to Figure 8a, increasing either CO_2 (Figure 8b) or H_2O (Figure 8c) partial pressure can enhance the gasification conversion. Moreover, in Figures 4 and 8, there is not much difference between the combustion and gasification rate. This is mainly because our combustion experiments are performed at 773, 823, and 873 K, while

https://doi.org/10.1021/acsomega.1c00131
ACS Omega 2021, 6, 9086−9094

gasification experiments are performed at 1273 K. In Figure 4, it takes about 12 min to finish combustion at 773 K, while only 5 min are required at 873 K. If the temperature increases to 1273 K, the time for finishing combustion would be much lower than 5 min and would be much faster than the gasification rate in Figure 8.

Figure 9 shows the gasification rate of different sampled chars. The difference in gasification rates originates from different gasification atmospheres. There is not much difference for the gasification rate of the sampled char at an atmosphere of 20% CO_2 + 20% H_2O (Figure 9a). A minor increase was observed for 2.0 min sampling char. The gasification rate obviously increases along with the sampling time at both 33.3% CO_2 + 20% H_2O (Figure 9b) and 20% CO_2 + 33.3% H_2O (Figure 9c).

As for the reaction index R_s from the overall average, char reactivity is shown in Figure 10. In Figure 10a, a minor decrease from 0.5 to 1.0 min sampling char is followed by the increase from 1.0 to 2.0 min sampling char. Overall, the difference of R_s in 20% CO_2 + 20% H_2O is not much. In Figure 10b, a minor decrease from 0.5 to 1.0 min sampling char is followed by a large increase from 1.0 to 2.0 min sampling char. In Figure 10c, R_s increases with the sampling time. Overall, in different gasification atmospheres, the reactivity of the sampled (partial gasified) char increases with the sampling time even though there is a minor decrease in the initial gasification stage. The same phenomenon can be found in the gasification reaction rate constant, as shown in Table 2. In Section 3.2, a reactivity decrease was observed in the late combustion stage in our combustion test, while it was not found in the gasification test probably due to the short sampling time in the MFB.

In gasification, a small amount (5%) of O_2 was injected together with CO_2/H_2O. In a low oxygen $O_2/CO_2/H_2O$ atmosphere, CO_2 concentration is high, which accelerates the char polycondensation reaction. Hence, gasification reactivity slightly decreases in the initial stage. Later, char pores become developed after initial gasification. The developed char structure results in the increase in the later gasification rate. Increasing CO_2 and H_2O (Figures 10b,c) concentrations in the gasification test further enhances the gasification reaction as well as reactivity. CO_2-enhanced gasification reactivity dominates for the highly gasified char, i.e. 1.5 and 2.0 min sampling char (Figure 10b). H_2O-enhanced gasification reactivity dominates for the low gasified char, i.e. 0.5 and 1.0 min sampling chars (Figure 10c).

4. CONCLUSIONS

In this study, we self-design an MFB with combination of an online char particle sampling system to study the kinetics of coal char combustion and gasification. For Vientiane coal, the online sampled char reactivity in the MFB obeys the rule of decrease−increase−decrease behavior with the sampling time. However, both pre-exponential factor A and activation energy E increase with the sampling time from the original char to sampled char. For the effects on the sampled char reactivity, the disordered char structure dominates in the early combustion stage (i.e., carbon conversion rate <10%); the pore structure dominates in the middle combustion stage (i.e., carbon conversion rate 10−60%); and the ash component dominates in the late combustion stage (i.e., carbon conversion rate >60%). In gasification, the reactivity of the sampled (partial gasified) char increases with the sampling time even though there is a minor decrease in the initial gasification stage. CO_2-enhanced gasification reactivity dominates for highly gasified char, while H_2O-enhanced gasification reactivity dominates for lowly gasified char. This study shows the reliability of the MFB combining online particle sampling to investigate char combustion and gasification, but the tests for different coal ranks as well as the application to other gas−solid reactions are certainly required in the future.

AUTHOR INFORMATION

Corresponding Authors

Zehua Li − *State Key Laboratory of Coal Combustion, School of Energy and Power Engineering, Huazhong University of Science and Technology, Wuhan, Hubei 430074, China; Department of Inorganic Chemistry, Fritz-Haber-Institut der Max-Planck-Gesellschaft, Berlin 14195, Germany;* orcid.org/0000-0003-2518-9287; Phone: +86-27-87545526; Email: lizehua90@163.com, lizehua@hust.edu.cn

Guangqian Luo − *State Key Laboratory of Coal Combustion, School of Energy and Power Engineering, Huazhong University of Science and Technology, Wuhan, Hubei 430074, China;* orcid.org/0000-0003-4697-4698; Phone: +86-27-87545526; Email: guangqian.luo@hust.edu.cn

Authors

Renjie Zou − *State Key Laboratory of Coal Combustion, School of Energy and Power Engineering, Huazhong University of Science and Technology, Wuhan, Hubei 430074, China;* orcid.org/0000-0003-3146-4716

Yang Xu − *Environment Research Institute, Shandong University, Qingdao 266237, China*

Liang Cao − *State Key Laboratory of Coal Combustion, School of Energy and Power Engineering, Huazhong University of Science and Technology, Wuhan, Hubei 430074, China*

Hong Yao − *State Key Laboratory of Coal Combustion, School of Energy and Power Engineering, Huazhong University of Science and Technology, Wuhan, Hubei 430074, China;* orcid.org/0000-0002-2836-7803

Complete contact information is available at: https://pubs.acs.org/10.1021/acsomega.1c00131

Notes

The authors declare no competing financial interest.

ACKNOWLEDGMENTS

This work is supported by the National Natural Science Foundation of China (grant no. 51776084), the National Key R&D Program of China (2018YFB0605100), and the China Postdoctoral Science Foundation (2018M632851). We also appreciate the Analytical and Testing Center of Huazhong University of Science and Technology for the provision of the testing instruments.

REFERENCES

(1) Toftegaard, M. B.; Brix, J.; Jensen, P. A.; Glarborg, P.; Jensen, A. D. Oxy-fuel combustion of solid fuels. *Prog. Energy Combust. Sci.* **2010**, *36*, 581−625.

(2) Buhre, B. J. P.; Elliott, L. K.; Sheng, C. D.; Gupta, R. P.; Wall, T. F. Oxy-fuel combustion technology for coal-fired power generation. *Prog. Energy Combust. Sci.* **2005**, *31*, 283−307.

(3) Li, Z.; Wang, Y.; Yao, H.; Lin, S. Novel CO_2 sorbent: $Ca(OH)_2$ with high strength. *Fuel Process. Technol.* **2015**, *131*, 437−442.
(4) Li, Z. H.; Wang, Y.; Xu, K.; Yang, J. Z.; Niu, S. B.; Yao, H. Effect of steam on CaO regeneration, carbonation and hydration reactions for CO_2 capture. *Fuel Process. Technol.* **2016**, *151*, 101−106.
(5) Li, Z.; Ouyang, J.; Luo, G.; Yao, H. High-efficiency CaO-based sorbent modified by aluminate cement and organic fiber through wet mixing method. *Ind. Eng. Chem. Res.* **2019**, *58*, 22040−22047.
(6) Wu, F.; Argyle, M. D.; Dellenback, P. A.; Fan, M. Progress in O_2 separation for oxy-fuel combustion-A promising way for cost-effective CO_2 capture: A review. *Prog. Energy Combust. Sci.* **2018**, *67*, 188−205.
(7) Tang, L.; Gupta, R.; Sheng, C.; Wall, T. The char structure characterization from the coal reflectogram. *Fuel* **2005**, *84*, 1268−1276.
(8) Lin, S.; Ding, L.; Zhou, Z.; Yu, G. Discrete model for simulation of char particle gasification with structure evolution. *Fuel* **2016**, *186*, 656−664.
(9) Zoulalian, A.; Bounaceur, R.; Dufour, A. Kinetic modelling of char gasification by accounting for the evolution of the reactive surface area. *Chem. Eng. Sci.* **2015**, *138*, 281−290.
(10) Li, T.; Zhang, L.; Dong, L.; Zhang, S.; Qiu, P.; Wang, S.; Li, C.-Z. Effects of gasification temperature and atmosphere on char structural evolution and AAEM retention during the gasification of Loy Yang brown coal. *Fuel Process. Technol.* **2017**, *159*, 48−54.
(11) Zhu, X.; Qian, W.; Li, X.; Tong, S.; Hu, Z.; Huang, Y.; Xia, A.; Yao, H. Moisture adsorption and spontaneous combustion characteristics of biomass wastes after degradative solvent extraction. *Fuel* **2020**, *266*, 117109.
(12) Ouyang, J.; Hong, D.; Jiang, L.; Li, Z.; Liu, H.; Luo, G.; Yao, H. Effect of CO_2 and H_2O on char properties. Part 1: pyrolysis char structure and reactivity. *Energy Fuels* **2020**, *34*, 4243−4250.
(13) Asadullah, M.; Zhang, S.; Min, Z.; Yimsiri, P.; Li, C.-Z. Importance of biomass particle size in structural evolution and reactivity of char in steam gasification. *Ind. Eng. Chem. Res.* **2009**, *48*, 9858−9863.
(14) Xu, J.; Liu, J.; Ling, P.; Zhang, X.; Xu, K.; He, L.; Wang, Y.; Su, S.; Hu, S.; Xiang, J. Raman spectroscopy of biochar from the pyrolysis of three typical Chinese biomasses: A novel method for rapidly evaluating the biochar property. *Energy* **2020**, *202*, 117644.
(15) Xu, J.; Tang, H.; Su, S.; Liu, J.; Xu, K.; Qian, K.; Wang, Y.; Zhou, Y.; Hu, S.; Zhang, A.; Xiang, J. A study of the relationships between coal structures and combustion characteristics: The insights from micro-Raman spectroscopy based on 32 kinds of Chinese coals. *Appl. Energy* **2018**, *212*, 46−56.
(16) Xu, Y.; Deng, F.; Pang, Q.; He, S.; Xu, Y.; Luo, G.; Yao, H. Development of waste-derived sorbents from biomass and brominated flame retarded plastic for elemental mercury removal from coal-fired flue gas. *Chem. Eng. J.* **2018**, *350*, 911−919.
(17) Xu, Y.; Zeng, X.; Luo, G.; Zhang, B.; Xu, P.; Xu, M.; Yao, H. Chlorine-Char composite synthesized by co-pyrolysis of biomass wastes and polyvinyl chloride for elemental mercury removal. *Fuel* **2016**, *183*, 73−79.
(18) Xu, Y.; Luo, G.; Zhang, Q.; Li, Z.; Zhang, S.; Cui, W. Cost-effective sulfurized sorbents derived from one-step pyrolysis of wood and scrap tire for elemental mercury removal from flue gas. *Fuel* **2021**, *285*, 119221.
(19) Lu, L.; Sahajwalla, V.; Harris, D. Coal char reactivity and structural evolution during combustion—Factors influencing blast furnace pulverized coal injection operation. *Metall. Mater. Trans. B* **2001**, *32*, 811−820.
(20) Liu, Y.; He, R. Modeling of the pore structure evolution in porous char particles during combustion. *Combust. Sci. Technol.* **2016**, *188*, 207−232.
(21) Davis, K. A.; Hurt, R. H.; Yang, N. Y. C.; Headley, T. J. Evolution of char chemistry, crystallinity, and ultrafine structure during pulverized-coal combustion. *Combust. Flame* **1995**, *100*, 31−40.
(22) Yu, J.; Guo, Q.; Ding, L.; Gong, Y.; Yu, G. Studying effects of solid structure evolution on gasification reactivity of coal chars by in-situ Raman spectroscopy. *Fuel* **2020**, *270*, 117603.
(23) Zhu, H.; Wang, X.; Wang, F.; Yu, G. In situ study on K_2CO_3-catalyzed CO_2 gasification of coal char: interactions and char structure evolution. *Energy Fuels* **2018**, *32*, 1320−1327.
(24) Fang, Y.; Zou, R.; Luo, G.; Chen, J.; Li, Z.; Mao, Z.; Zhu, X.; Peng, F.; Guo, S.; Li, X.; Yao, H. Kinetic study on coal char combustion in a microfluidized bed. *Energy Fuels* **2017**, *31*, 3243−3252.
(25) Jiang, L.; Li, Z.; Ouyang, J.; Fang, Y.; Luo, G.; Yao, H. Kinetic study of coal char thermal deactivation. *Energy Fuels* **2019**, *33*, 11959−11967.
(26) Li, Z.; Zou, R.; Hong, D.; Ouyang, J.; Jiang, L.; Liu, H.; Luo, G.; Yao, H. Effect of CO_2 and H_2O on char properties. Part 2: *in situ* and *ex situ* char in oxy-steam combustion. *Energy Fuels* **2020**, *34*, 7554−7563.
(27) Chen, C.; Zhang, S.; Xu, K.; Luo, G.; Yao, H. Experimental and modeling study of char gasification with mixtures of CO_2 and H_2O. *Energy Fuels* **2016**, *30*, 1628−1635.
(28) Chen, C.; Wang, J.; Liu, W.; Zhang, S.; Yin, J.; Luo, G.; Yao, H. Effect of pyrolysis conditions on the char gasification with mixtures of CO_2 and H_2O. *Proc. Combust. Inst.* **2013**, *34*, 2453−2460.
(29) Zou, R.; Cao, L.; Luo, G.; Li, Z.; Sun, R.; Li, X.; Yao, H. Pretreatment of petroleum coke to enhance the reactivity of catalytic gasification in fluidized beds. *Energy Fuels* **2018**, *32*, 8115−8120.
(30) Guo, Y.; Zhao, Y.; Gao, D.; Liu, P.; Meng, S.; Sun, S. Kinetics of steam gasification of in-situ chars in a micro fluidized bed. *Int. J. Hydrogen Energy* **2016**, *41*, 15187−15198.
(31) Feng, D.; Guo, D.; Zhao, Y.; Zhang, Y.; Geng, K.; Chang, G.; Sun, S. In-situ decoupling effect of H_2O on the whole process of coal gasification in MFBRA and TG-FTIR-MS. *J. Anal. Appl. Pyrolysis* **2020**, *145*, 104744.
(32) Wang, F.; Zeng, X.; Geng, S.; Yue, J.; Tang, S.; Cui, Y.; Yu, J.; Xu, G. Distinctive hydrodynamics of a micro fluidized bed and its application to gas−solid reaction analysis. *Energy Fuels* **2018**, *32*, 4096−4106.
(33) Zeng, X.; Kahara, K.; Ueki, Y.; Yoshiie, R.; Xu, G.; Naruse, I. Characteristics of biomass devolatilization and in situ char gasification tested by the non-isothermal method. *Energy Fuels* **2019**, *33*, 9805−9817.
(34) Horn, R.; Degenstein, N. J.; Williams, K. A.; Schmidt, L. D. Spatial and temporal profiles in millisecond partial oxidation processes. *Catal. Lett.* **2006**, *110*, 169−178.
(35) Horn, R.; Korup, O.; Geske, M.; Zavyalova, U.; Oprea, I.; Schlögl, R. Reactor for in situ measurements of spatially resolved kinetic data in heterogeneous catalysis. *Rev. Sci. Instrum.* **2010**, *81*, No. 064102.
(36) Korup, O.; Mavlyankariev, S.; Geske, M.; Goldsmith, C. F.; Horn, R. Measurement and analysis of spatial reactor profiles in high temperature catalysis research. *Chem. Eng. Process.* **2011**, *50*, 998−1009.
(37) Daniel, C.; Clarté, M. O.; Teh, S.-P.; Thinon, O.; Provendier, H.; Van Veen, A. C.; Beccard, B. J.; Schuurman, Y.; Mirodatos, C. Spatially resolved catalysis in microstructured reactors by IR spectroscopy: CO oxidation over mono- and bifunctional Pt catalysts. *J. Catal.* **2010**, *272*, 55−64.
(38) Li, Z.; Jiang, L.; Ouyang, J.; Cao, L.; Luo, G.; Yao, H. A kinetic study on char oxidation in mixtures of O_2, CO_2 and H_2O. *Fuel Process. Technol.* **2018**, *179*, 250−257.
(39) Ye, D. P.; Agnew, J. B.; Zhang, D. K. Gasification of a South Australian low-rank coal with carbon dioxide and steam: kinetics and reactivity studies. *Fuel* **1998**, *77*, 1209−1219.
(40) Molina, A.; Mondragón, F. Reactivity of coal gasification with steam and CO_2. *Fuel* **1998**, *77*, 1831−1839.
(41) Sadhukhan, A. K.; Gupta, P.; Saha, R. K. Modelling of combustion characteristics of high ash coal char particles at high pressure: Shrinking reactive core model. *Fuel* **2010**, *89*, 162−169.

https://doi.org/10.1021/acsomega.1c00131
ACS Omega 2021, 6, 9086−9094

(42) Sadhukhan, A. K.; Gupta, P.; Saha, R. K. Analysis of the dynamics of coal char combustion with ignition and extinction phenomena: Shrinking core model. *Int. J. Chem. Kinet.* **2008**, *40*, 569−582.

https://doi.org/10.1021/acsomega.1c00131
ACS Omega 2021, 6, 9086−9094